Journal of Electroanalytical Chemistry 731 (2014) 28–35

Contents lists available at ScienceDirect

Journal of Electroanalytical Chemistry

journal homepage: www.elsevier.com/locate/jelechem

Electrochemical oxygen reduction at soft interfaces catalyzed by the transfer of hydrated lithium cations

Haiqiang Deng [a,1], T. Jane Stockmann [a,1], Pekka Peljo [a], Marcin Opallo [b], Hubert H. Girault [a,*]

[a] Laboratoire d'Electrochimie Physique et Analytique, Ecole Polytechnique Fédérale de Lausanne (EPFL), Station 6, CH-1015 Lausanne, Switzerland[2]
[b] Institute of Physical Chemistry, Polish Academy of Sciences, ul. Kasprzaka 44/52, 01-224 Warszawa, Poland

ARTICLE INFO

Article history:
Received 17 June 2014
Received in revised form 28 July 2014
Accepted 31 July 2014
Available online 8 August 2014

Keywords:
ITIES
Oxygen reduction reaction
Decamethylferrocene
Lewis acid catalyzed
Lithium
Liquid|liquid electrochemistry

ABSTRACT

The oxygen reduction reaction by decamethylferrocene (DMFc), triggered by hydrophilic metallic cations behaving as Lewis acids towards water molecules in a homogeneous organic phase reaction, was investigated using cyclic voltammetry at the water|1,2-dichloroethane (w|DCE) interface. Simulated CVs, prepared through a facile 1-dimensional geometry in COMSOL Multi-physics software and incorporating interfacial and homogeneous reactions, were compared to experimental ones in order to elucidate the kinetics, thermodynamics, and viability of the proposed mechanism. The predominant O_2 reduction reactions were proposed to occur in bulk organic phase, or in the vicinity of the w|DCE interface; six organic phase reactions were put forward. The first step was hydrolysis made possible through polarization of the O—H bond of water molecules available in the cations hydration shell. The metal ion behaves as a Lewis acid coordinating to the oxygen and weakening the O—H bond, making the proton more acidic, thereby facilitating attack by decamethylferrocene (DMFc) to form DMFc-H^+. DMFc-H^+ then participates in dioxygen reduction, generating the $O_2H^{\cdot}$ radical species and $DMFc^+$. Afterwards, the radical oxidizes another equivalent of DMFc to produce O_2H^-, that can then abstract a proton from the metal ions hydration sphere to generate hydrogen peroxide. The disproportionation of O_2H^- and the ion-pair formation of Li^+ and OH^- make up the other two reactions. The CV analysis was based on two curve features; the $DMFc^+$ transfer wave and the positive limit of the polarizable potential window – the edge of scan potential profile – including the metal ion return peak. The goal of this article is to determine the kinetic/thermodynamic aspects of this mechanism from the experimental electrochemical data.

1. Introduction

The oxygen reduction reaction (ORR) at metal surfaces [1–4], in solution [2,5–8], and in biological systems is of considerable importance as it impacts solid electrode performance and is an integral reaction for fuel cells and artificial photosynthesis [9]. In the case of hydrogen fuel cells, poor O_2 reduction kinetics elicit appreciable overpotentials that greatly limit the power outputs [2] of the device stimulating interest in mechanistic and kinetic characterization of this reaction. To that end, the ORR has been extensively studied in organic and aqueous systems, while recently expanding to include novel solvents such as ionic liquids [10,11]. At the same time, a great deal of research has been directed towards the development of new, cheaper catalysts such as metal-porphyrins [12–14]. In the past 10 years non-heme iron(IV)-oxo catalysts have come under attention [15–17], and it has been demonstrated that polymer based cathodes incorporating these catalysts were comparable to traditional Pt cathodes.

Simultaneously, oxygen reduction has been characterized at the interface between two immiscible electrolytic solutions (ITIES) [5–7,18–25], often between water and an organic solvent (e.g., 1,2-dichloroethane, DCE). Electrochemistry at an ITIES has several advantages over conventionally solid/liquid methods. For example, the liquid|liquid interface is intrinsically defect free; therefore, it does not require the extensive polishing associated with solid electrodes. Additionally, the water and organic phases can be treated as a convenient means for product or reagent separation – in some cases facilitating charge separation – while early studies focused on evaluating porphyrin-based catalysts [18,26].

Regardless of which system is employed – solid/electrolyte [2,3,14,16], liquid|liquid [5,8,13,18–21,23–25,27,28], or homogeneous [7,8,12,22] – or which catalyst is used, an electrode or an electron donor, which can be sacrificial, is typically required. Here,

* Corresponding authors. Tel.: +41 21 693 3145; fax: +41 21 693 3667.
E-mail address: hubert.girault@epfl.ch (H.H. Girault).
[1] These authors contributed equally to this work.
[2] http://lepa.epfl.ch/.

http://dx.doi.org/10.1016/j.jelechem.2014.07.040
1572-6657/

decamethylferrocene (DMFc), 1,1′-dimethylferrocene (DFc), or ferrocene (Fc) are used as organic electron donors. Samec et al. reported that significant changes in the rate of the ORR reaction could take place depending on which electron donor was utilized [28]. They also reported a strong inhibition of a cobalt-porphyrin catalyzed ORR through a proposed coordination of H_2O to the cobalt center in a homogeneous organic phase experiment [5]. Additionally, it has been discovered that sufficiently strong electron donors, like many ferrocene derivatives, could perform O_2 reduction independently in the absence of a catalyst, when protons are available, albeit much slower [6,20,22,24,27]. A mechanism was then proposed based on spectroscopic and kinetic/thermodynamic evidence for the DMFc, water|DCE (w|DCE) case [6,20,22]. First, the proton undergoes ion transfer from water (w) to organic (o) phase where it then binds to the metal center of DMFc forming the DMFc-hydride ($DMFc\text{-}H^+$) [6,20,22]. $DMFc\text{-}H^+$ subsequently reacts with dissolved O_2 to form $DMFc^+$ and the hydrogen peroxyl radical, $O_2H^{\cdot}$ [6,20,22]. $O_2H^{\cdot}$ can oxidize one equivalent of DMFc to form $DMFc^+$ and O_2H^-, which can then either become protonated to form H_2O_2 or disproportionate to form dioxygen and two equivalents of OH^-.

This is one possible O_2 reduction mechanism, as recently outlined by Girault et al. [6]; however, a novel mechanism, utilizing alkali metals in the absence of an acid, has recently been evidenced [7], in which water – dissolved in the organic phase – becomes the proton source in a Lewis acid catalyzed reaction. Through this pathway [7], the alkali, or other metal ion, transfers from the aqueous to organic phase – either into a hydration pocket, as has been shown [29], or with some of its hydration sphere intact. The metal ion, coordinating to the oxygen of the surrounding H_2O molecules, weakens the O—H bonds within the hydration sphere and facilitates the abstraction of a proton by DMFc to form $DMFc\text{-}H^+$ [7]. In this way, the metal ion behaves as a Lewis acid with the subsequent proposed mechanistic steps mirroring those of the previous acid catalyzed pathway.

Metals, particularly transition metals, behaving as Lewis acids have been used to catalyze synthetic reactions with significant architectures [30] or stereochemistry for decades [31]. Fukuzumi et al. have recently demonstrated that the reactivity of the Fe(IV) = O moiety within the non-heme iron(IV)-oxo catalysts – when used for C-bond cleavage – can be enhanced through the presence of Lewis acids such as triflic acid or scandium(III) triflate [32]. While this Lewis acid behaviour is generally well known, its incorporation into DMFc mediated O_2 reduction is novel [7].

The goal of the present work is to consolidate the electrochemical evidence acquired at biphasic (in this case w|DCE) systems obtained through cyclic voltammetry (CV), with previous spectroscopic (mass spectroscopy, UV/Vis, etc.) observations [7] and elucidate the kinetics/thermodynamics of Lewis acid catalyzed O_2 reduction at liquid|liquid interfaces. To achieve this, COMSOL Multi-physics was employed utilizing a facile 1-dimensional geometry of the w|DCE interface (millimeter scale), to generate simulated CVs. By altering the rates of the different reaction steps, recording the resultant changes in the simulated CV, and then comparing them to the experimental ones, the mechanism proposed herein was investigated.

2. Simulations

Simulation software, like COMSOL Multi-physics, which employs the finite element method, has been used to evaluate a broad spectrum of phenomenon including nanocrystalline phase change memory cells [33], the thickness of methanol fuel cell cathode catalyst layers [34], hydrogen storage tanks [35], nuclear fuel bundles [36], and a host of electrochemical phenomenon [37–39]; the latter has been subject to a recent mini-review concerning electrochemical analysis [40]. Herein, this versatile software was used to explore the mechanism and kinetics of O_2 reduction in water|organic solvent (w|o), biphasic systems. The model, comprised of a facile 1-dimensional geometry depicted in Fig. 1, contained two subdomains to represent either phase and three boundaries. The boundaries at the terminal ends of the geometry in Fig. 1 were given the designation 'concentration' in the software, which is used to describe the bulk concentration of species unaffected during the time scale of the experiment. Mass transport, for the fully supported electrolyte solution, was described within each phase using Fick's laws as per the following equation,

$$\frac{\partial c_{i,w}(x,t)}{\partial t} = D_{i,w}\nabla c_{i,w}(x,t) = D_{i,w}\left(\frac{\partial^2 c_{i,w}(x,t)}{\partial^2 x}\right) \quad \text{(i)}$$

for a 1-dimensional system, such that $c_{i,w}$ and $D_{i,w}$ are the concentration and diffusion coefficient of species i in water (w); an analogous equation can be written for the organic (o) phase. A model incorporating the Nernst–Planck series of equations describing mass transport, which take into account diffusion along with migration, was considered. However, migration was deemed a small contributor at experimental, electrolyte concentrations to the overall current density; furthermore, the complexity of programming such a system was found to be prohibitive. Therefore a more facile simulation employing only Fick's laws was considered moving forward.

Potential dependent ion transfer (IT) across the central boundary (Fig. 1) of an ion, with a charge z_i, can be written as:

$$I_w^{z_i} \rightleftharpoons I_o^{z_i} \quad \text{(ii)}$$

IT was controlled using Butler–Volmer kinetics described by the forward and reverse, k_f and k_b, rate constants, respectively, through the following:

$$k_f = k^o \exp(-\alpha f(\Delta_o^w\phi - \Delta_o^w\phi^{o\prime}) \quad \text{(iii)}$$

$$k_b = k^o \exp((1-\alpha) f(\Delta_o^w\phi - \Delta_o^w\phi^{o\prime}) \quad \text{(iv)}$$

where k^o is the standard rate constant (a value of 1 cm s^{-1} was used unless otherwise noted for fully reversible IT), α is the transfer coefficient (0.5 was used throughout), and f is F/RT, where F is Faraday's constant, R is the universal gas constant, and T is temperature. $\Delta_o^w\phi$ is the Galvani potential difference across the interface, $\phi_w - \phi_o = \Delta_o^w\phi$, and was approximated using a triangular waveform [39,41] in order to mirror the CV experiments. A formal IT potential, $\Delta_o^w\phi_i^{o\prime}$, of 0.696 V, described for lithium cations [42] at the w|DCE interface, was used throughout unless otherwise stated.

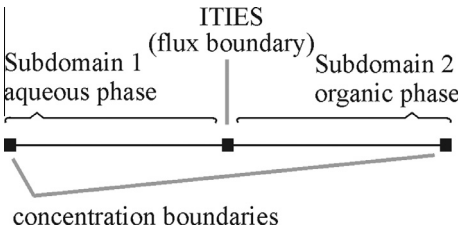

Fig. 1. The 1-dimensional simulation geometry (thin black line) with three boundaries (squares) as drawn in COMSOL Multi-physics software. The geometry was split into subdomains 1 and 2 representing the aqueous and organic phases, respectively, within which mass transport was governed by Fick's laws of diffusion. The outer boundaries were given the designation 'concentration' in the software, representing the bulk solution beyond which point the solution concentration profile is not expected to change on the time scale of the experiment. The interface between two immiscible electrolytic solutions (ITIES), shown at center, was given the boundary condition 'flux', such that species could cross the interface either through ascribed partition coefficients or through potential dependent ion transfer described by Butler–Volmer kinetics.

The current was taken to be the sum of the flux of charged species across the ITIES via [43]:

$$J(x,t) = FA\sum_i z_i D_{i,w} \nabla c_{i,w}(x,t) \quad (v)$$

where A is the electrode area as defined by a circle of radius 0.7 cm. The simulation mesh was validated using simple IT and comparison of the peak current to the Randles–Sevčik equation [43,44] as demonstrated recently [6].

3. Experimental methods

3.1. Chemicals

All chemicals were of analytical grade and employed without further purification save for decamethylferrocene (DMFc , Alfa Aesar GmbH), which was purified by vacuum sublimation at 140 °C. Ferrocene (Fc, 98%) and molybdenum carbide (Mo_2C, ~325 mesh, ⩾99.5%) were purchased from Aldrich, while lithium tetrakis(pentafluorophenyl)borate diethyl etherate (LiTB) was obtained from Boulder Scientific (Longmont, CO). Sodium chloride (NaCl), sodium iodide (NaI), bis(triphenylphosphoranylidene) ammonium chloride (BACl), 1,2-dichloroethane (DCE), tetraethylammonium chloride (TEACl, ⩾98%), and tetramethylammonium sulfate (TMA_2SO_4) were sourced from Fluka. Bis(triphenylphosphoranylidene) ammonium tetrakis(pentafluorophenyl)borate (BATB) was prepared by metathesis of 1:1 mixtures of BACl and LiTB, in a methanol/water (v/v = 2) mixture, followed by recrystallization in acetone. A Millipore-Q filtration system (Merck Millipore, Billerica, MA) was used to generate ultrapure water (18.2 MΩ cm) from which all aqueous solutions were prepared.

3.2. Instrumentation

3.2.1. Four-electrode liquid/liquid interface voltammetry

CV measurements were recorded through the use of a PGSTAT30 potentiostat (Metrohm, CH) at the w|DCE interface via three-compartment, four-electrode glass cell [45–47]. Two quasi-reference electrodes, one immersed in the aqueous phase and another in DCE, were introduced close to the ITIES through the use of Luggin capillaries, and used to measure the polarization of the interface (geometric area of 1.53 cm^2). Two counter electrodes positioned in the water and organic phases were employed to complete the electric circuit and monitor the interfacial current. The following electrochemical cell was used:

$$\mathrm{Ag}\,|\,\mathrm{AgOH}\,|\,\underset{(aq)}{\text{10 mM LiOH}}\,\|\,\underset{(DCE)}{\text{5 mM 'Fc deriv.' 5 mM BATB}}\,|\,\underset{(aq\sim ref.)}{\text{10 mM LiCl 1 mM BACl}}\,|\,\mathrm{AgCl}\,|\,\mathrm{Ag} \quad \text{(Cell 1)}$$

(Cell1)

LiOH was employed as the supporting electrolyte/analyte in aqueous phase, while BATB served as the supporting electrolyte in the organic phase. 'Fc deriv.' refers to the three ferrocene derivatives evaluated individually; Fc, DFc, and DMFc. The potential scale was calibrated through the use of the tetraphenylarsonium-tetraphenylborate (TATB) [45–47], or Parker's [48,49] assumption and the addition of an ion of known standard IT potential; in this case, tetramethylammonium (TMA^+, $\Delta_o^w\phi^{o'}_{TMA^+} = 0.160$ V) or tetraethylammonium (TEA^+, $\Delta_o^w\phi^{o'}_{TEA^+} = 0.019$ V) ion transfer was used [50].

All experiments were performed under aerobic – open benchtop – conditions, such that any oxygen consumed by reactions in either phase could be readily replenished.

3.2.2. Computations

All simulations were performed using a MacIntosh computer with 4 Intel Xeon(R) 5150 processors operating at 2.66 GHz and using the Ubuntu 12.04 LTS operating system; runtimes ranged from 15 to 18 min.

4. Results and discussion

Fig. 2 illustrates CVs obtained using Cell 1 with (solid trace) or without (dashed curve) 5 mM of DMFc in the organic phase. The polarizable potential window (PPW) was swept at 0.050 V s^{-1} with a potential range of ±0.530 V.

To obtain the blank CV in Fig. 2, the potential was initially swept from 0.000 to 0.530 V at a scan rate of 0.050 V s^{-1} until a sharp rise in the current density was reached at 0.530 V; at which point the scan direction was reversed and proceeded towards more negative potentials. The sharp increasing current is owing to the transfer of the supporting electrolyte ions, Li^+ (from w to o) and TB^- (from o to w) and represents the positive limit of the polarizable potential window (PPW). Next, the potential was swept from 0.530 to −0.530 V; initially the current density decreases rapidly followed by a negative peak-shaped wave at ~0.400 V that is indicative of the return of Li^+ from o to w and TB^- from w to o. The scan was continued until roughly −0.500 V when a sharp decrease in the current density was observed. This is representative of IT of the other supporting electrolyte components; specifically, the transfer of OH^- (from w to o) and BA^+ (from o to w) – the transfer of these ions constitutes the negative potential limit of the PPW. Similar to Li^+ and TB^-, a positive return peak was recorded, when the potential was swept from −0.530 to 0.000 V, and represents the transfer of OH^- and BA^+ back across the interface. It is likely, however, that TB^- and BA^+ are minor contributors to the current signal at the PPW limit owing to their large hydrophobicity [42,51].

The solid trace in Fig. 2 describes the system after addition of DMFc to the organic phase; an IT wave was recorded with a half-wave potential of −0.338 V that is indicative of the transfer of $DMFc^+$, and its transfer potential is in fair agreement with previous reports [6,7,21,27]. The appearance of the $DMFc^+$ transfer wave is somewhat surprising and the signal intensity is beyond that expected from simple contamination of the stock DMFc, which is common in commercial sources of this reagent [6]. The oxidation of DMFc has been known to take place in acidic media through the ORR [5,20,23–25,27]; however, as recently demonstrated [7], DMFc oxidation via ORR can take place in alkaline solutions, albeit at reduced rates of reaction. Additionally, comparing the blank

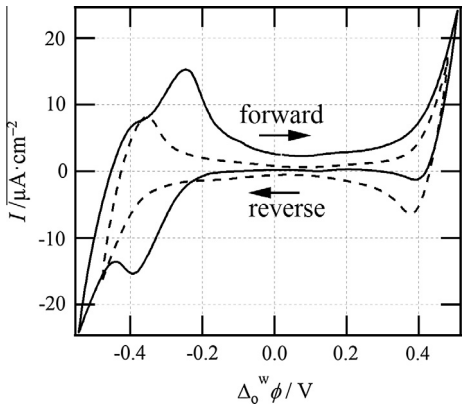

Fig. 2. Experimental cyclic voltammograms obtained using Cell 1 under aerobic conditions with (solid trace) and without (dashed curve) 5 mM of DMFc added to the organic phase. Instrument parameters included a scan rate of 0.050 V s^{-1} with a potential range of approximately ±0.530 V.

(dashed) curve without DMFc and the solid curve with DMFc added, a decrease in the Li^+ return peak intensity, from −6.393 to −3.358 μA cm^{-2} (baseline corrected), respectively, was observed. This suggests that metal ions may be either sequestered or consumed in a process that generates $DMFc^+$. Similar experiments were performed under anaerobic conditions in a glove-box (data not shown), with no change between the blank and DMFc added cases. It may be worthy to mention that ferrocene is stable in alkaline media [52] and so it can be expected that DMFc should also be resistant to basic conditions – at least on the time scale of these experiments.

It was also demonstrated recently [6] in CV experiments obtained at a the liquid|liquid interface, where H_2SO_4 was employed as both supporting electrolyte and analyte, that the current density-potential profile at the positive end of the PPW, along with the peak intensity of the $DMFc^+$ transfer wave (or other oxidized Fc derivative) could be used as measures towards the kinetics of ORR. In that submission [6], a correlation between a decrease in the H^+ return-peak intensity and increase in IT wave intensity of the oxidation product of an electron donor in the organic phase (*e.g.* a Fc derivative) was recognized. In this way, a mechanism was tested [6] wherein protons were consumed in a series of reactions that reduced dioxygen to hydrogen peroxide, or water, while oxidizing DMFc.

In a similar manner, the mechanism drawn in Fig. 3 has been proposed, such that a metal ion crosses the ITIES – owing to the applied Galvani potential difference – but because of its hydrophilicity, the metal ion retains some of its hydration sphere, or is transferred into hydration pockets within the organic phase as described by Mirkin et al. [29]. In this way, the metal ion is closely associated with H_2O in the organic phase and can behave as a Lewis acid through coordination of the metal ion to the oxygens within the surrounding water molecules. The metal ion can then weaken the O—H bond and, thus, water becomes the proton source for oxygen reduction – similar to oxygen reduction in alkaline conditions.

The homogeneous reactions outlined in Fig. 3 were incorporated into the simulation model described in Section 2. In this system interfacial reactions included the potential dependent IT of Li^+, OH^-, and $DMFc^+$, as described through Butler–Volmer kinetics, along with the non-potential dependent partition of the neutral ion pair MOH. These were coupled with the bulk organic phase reactions **1** to **6**. For simplicity, this study has limited itself to these six reactions. In reaction **1**, as shown below, DMFc abstracts a proton from water in the hydration sphere of the metal ion.

$$DMFc + M^+(H_2O)_m \underset{k_{cb}}{\overset{k_{cf}}{\rightleftharpoons}} DMFc - H^+ + M^+(OH)^-(H_2O)_{m-1} \quad (1)$$

The number of water molecules within the inner metal ion hydration sphere, m, is highly dependent on the ion under consideration; it has been shown to be as much as $m = 8$ for Rb^+ and Cs^+, while Li^+ and Na^+ exhibit values of 4 and 5 to 6, respectively, such that m is highly correlated to the ionic radius of the metal ion [53]. DMFc has been shown to form DMFc-hydrides in acidic media [7,20,22,27,28] and is an electron donor for O_2 reduction and hydrogen evolution reactions. Reaction **1** is an equilibrium reaction where the forward and reverse reactions are described by the rate constants designated in the simulation as k_{cf} and k_{cb}, respectively.

In acidic conditions, the proton has been found to coordinate to the DMFc metal center, which is then available for reaction with O_2 to ultimately produce hydrogen peroxide through a series of reactions [22]; this mechanism is supported by density functional theory calculations. With this in mind, reaction **2** was chosen, as detailed below, such that O_2 reacts with DMFc-H^+ to from $DMFc^+$ and the hydrogen peroxyl radical, $HO_2^{\cdot}$.

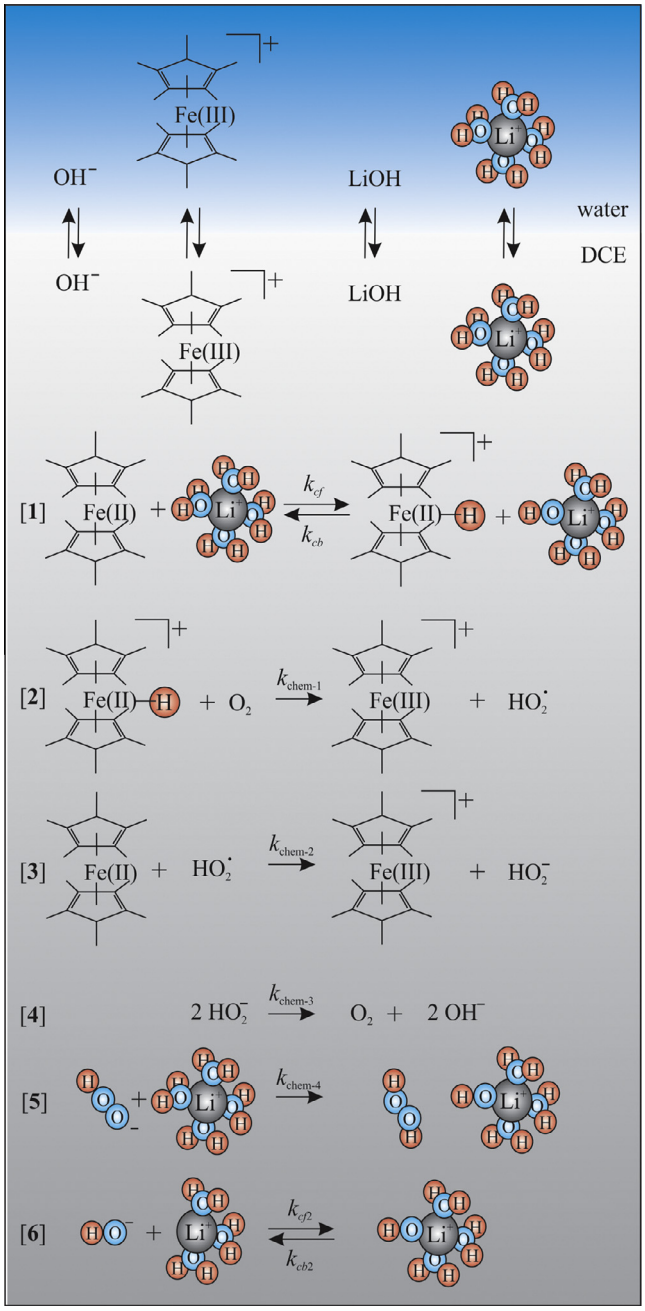

Fig. 3. Proposed mechanism of Li^+ Lewis acidity at a w|DCE interface.

$$DMFc - H^+ + O_2 \overset{k_{chem-1}}{\rightarrow} DMFc^+ + HO_2^{\cdot} \quad (2)$$

Reactions **3** and **4**, described by the rate constants k_{chem-2} and k_{chem-3}, respectively, and given below, illustrate one possible fate for $HO_2^{\cdot}$, in that it reacts with one equivalent to DMFc to generate $DMFc^+$ and HO_2^-. The latter subsequently disproportionates to oxygen and OH^-, or alternatively, HO_2^- can react in a similar manner as DMFc and abstract a hydrogen from the hydration sphere of the metal ion forming hydrogen peroxide; this pathway was included through reaction **5** and governed by the rate constant k_{chem-4}.

$$DMFc + HO_2^{\cdot} \overset{k_{chem-2}}{\rightarrow} DMFc^+ + HO_2^- \quad (3)$$

$$2HO_2^- \overset{k_{chem-3}}{\rightarrow} O_2 + 2OH^- \quad (4)$$

$$2HO_2^- + M^+(H_2O)_m \xrightarrow{k_{chem-4}} H_2O_2 + M^+(OH^-)(H_2O)_{m-1} \quad (5)$$

The final bulk reaction under consideration was the formation of the metal ion-hydroxide ion-pair as given through reaction **6**:

$$M^+ + OH^- \underset{k_{cb2}}{\overset{k_{cf2}}{\rightleftharpoons}} [M^+OH^-] \quad (6)$$

The association constant, K_f, can be related to the forward and reverse rate constants, k_{cf2} and k_{cb2}, respectively, through the following:

$$\frac{k_{cf2}}{k_{cb2}} = K_f = \frac{c_{[M^+OH^-]}}{c_{M^+}c_{OH^-}} \quad (vi)$$

Reaction **6** was active in both aqueous and organic phases, such that the ion-pair formation is favoured (high k_{cf2}) and disfavoured (high k_{cb2}) in o and w, respectively. This is in keeping with the Bjerrum and Fuoss models which describe the association constant for ion-pair formation as decreasing with increasing dielectric constant [54]. In this case, the high and low dielectric constant in water and DCE, 78.4 and 10.2 [55], discourage and promote ion-pair formation, respectively. The organic phase ion-pair association constant was an additional parameter investigated through the simulation.

Moving forward, the simulation was performed using the parameters given in Table S1, of the Supplementary Data, while varying the rates of reaction **1** to **6**. Fig. 4 contains plots of simulated CVs where k_{chem-1}, k_{chem-2}, k_{chem-3}, and k_{chem-4} were all maintained at 1×10^4 L mol^{-1} s^{-1}, k_{cb} was set equal to 1 s^{-1}, and k_{cf} was varied from 1×10^2 L mol^{-1} s^{-1} to 1×10^5 and 1×10^8 L mol^{-1} s^{-1} for Fig. 4 A, B, and C, respectively.

As the rate of **1** increases through A, B, and C, the peak current density for the transfer of $DMFc^+$ increases from -2.06 μA cm^{-2} to -17.5 and -905 μA cm^{-2}, respectively. Simultaneously, the return peak for metal IT at 0.510 V in panel A of Fig. 4 was -1.3 μA cm^{-2}, but is not present in traces B or C. Indeed, in Fig. 4C a peak-shaped wave has emerged on the forward scan at 0.470 V with a peak current density of 2200 μA cm^{-2}. This peak is similar to the voltammetric response for facilitated IT using ligands, or ionophores,

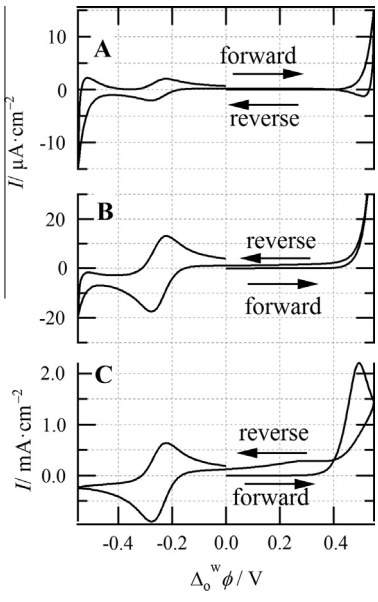

Fig. 4. Simulated cyclic voltammograms generated using COMSOL Multi-physics using the 1-dimensional geometry illustrated in Fig. 1 and the simulation parameters listed in Table S1 (Supplementary Data); however, with k_{chem-1}, k_{chem-2}, k_{chem-3}, and k_{chem-4} were set equal to 1×10^4 L mol^{-1} s^{-1}, while k_{cb} was set equal to 1 s^{-1}. k_{cf} was varied from 1×10^2 to 1×10^5 and 1×10^8 L mol^{-1} s^{-1} for panels A, B, and C, respectively.

through a conventional EC (electrochemical-chemical) or TOC (transfer of the metal ion, followed by organic phase complexation) mechanism as described recently by Molina et al. [56] and classically by Mareček et al. [57] as well as Girault et al. [58]. In the present model, IT serves as the electrochemical step, whilst proton transfer to the metal center of DMFc – to form DMFc-H^+ – is the chemical step. The latter is analogous to a complexation reaction; however, here the metal ion is acting as a Lewis acid – essentially behaving as a catalyst for hydride formation. In traditional complexation reactions across the ITIES with an increasing complexation constant, the transfer potential of a metal cation (transferring from w to o) decreases, or shifts towards more negative potentials [56]. In this way, the model is in good agreement with the present understanding of facilitated IT [56–58] at liquid|liquid interfaces.

In Fig. 4B, the current density during the forward scan is lower than that observed during the reverse scan, while normally, and in Fig. 4A, this is reversed. For Fig. 4C, this effect is more exaggerated and a positive peak current density response was even observed at 0.295 V. By examining the concentration profiles (data not shown) it was found that the flux of OH^-, from o to w, was responsible. It was also found that the facilitated IT of the metal ion, through the TOC mechanism, was not limited by the diffusion of either the metal ion or DMFc, but rather was sequestered as an ion-pair in the organic phase. In the present model, MOH is not catalytic; therefore, the ion-pair formation would block any further O_2 reduction. The rate constants used in Fig. 4B and C are high relative to other ORR rate constants reported in the literature [28] and have been used here to demonstrate an extreme case. The CV response plotted in Fig. 4A is replicates more accurately the experimental data given in Fig. 2; however, the peak current density for $DMFc^+$ is much lower (by a factor of 5) in the simulated results. This discrepancy between the experimental and simulated peak current density for the IT wave of $DMFc^+$ may be owing to a number of factors arising from the experiment. For example, when conducting the experiment often multiple voltammetric scans are necessary to establish a potential window and this would result in a buildup of $DMFc^+$ near the interface – artificially enhancing its IT response. Additionally, owing to instabilities in the current density-potenital profile, multiple CVs are necessary in order to acquire a clean trace for good comparison; these instabilities are sometimes referred to as the Marangoni effect [59], and are thought to be caused by an assortment of phenomena including spontaneous emulsification, changes in interfacial surface tension, etc. To compound this, if the experiment is allowed to stand for a period of time the reaction may proceed; however, owing to the high hydophilicity of Li^+ this can be considered a minor contributor.

Subsequently, the rate of reaction **2**, the formation of $DMFc^+$, was examined. At this stage, a k_{cf} equal to 1×10^3 L mol^{-1} s^{-1} was used and k_{chem-1} was varied from 1×10^2 L mol^{-1} s^{-1} to 1×10^4 and 1×10^8 L mol^{-1} s^{-1}, as shown in Fig. 5, such that the resultant cathodic peak current density for the $DMFc^+$ transfer wave was observed to be -7.5, -25.7, and -25.9 μA cm^{-2}, respectively. This indicates that, despite reaction **1** being rate limiting, increasing the rate of **2** can still elicit an increase in product formation; however, large rate increases are necessary with depreciating returns in the $DMFc^+$ generation. During the forward sweep of the simulated CVs where k_{chem-1} was 1×10^4 and 1×10^8 L mol^{-1} s^{-1}, the current density remains close to baseline until the edge of the PPW was reached and a sharp increase, associated with the transfer of Li^+ from w to o, was recorded. However, upon reversal of the scan direction (from 0.550 to -0.550 V) the rapid decrease in the current density seen experimentally was not observed. Instead, a gradual decline in the current density was obtained; this was associated with the flux of OH^- – generated through reactions **1**, **4**, and **6** – from o to w. This current density offset was observed

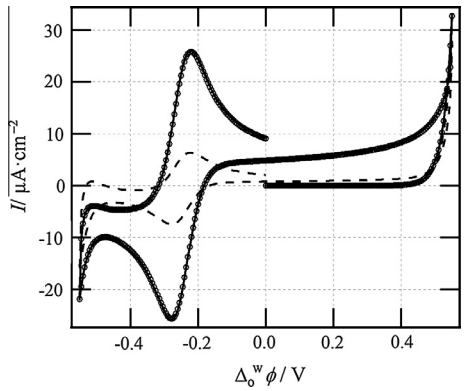

Fig. 5. Cyclic voltammograms obtained via simulation using similar conditions as described for Fig. 4; however, $k_{cf} = 1 \times 10^3$ L mol^{-1} s^{-1} was employed whilst varying $k_{chem\text{-}1}$ to 1×10^2 (dashed line), 1×10^4 (○), and 1×10^8 L mol^{-1} s^{-1} (solid line).

but not reproducible experimentally but may be the cause of slight positive potential shift observed across the entire CV in Fig. 2 after addition of DMFc; however, $k_{chem\text{-}1}$ values greater than 1×10^4 L mol^{-1} s^{-1} should not be considered.

Subsequently Fig. 6 was generated and illustrates the investigation of the metal-ion-hydroxide ion-pair formation in the organic phase on the CV response using the parameters given in Table S1. k_{cf2} was set equal to 5000 L mol^{-1} s^{-1}, while k_{cb2} was changed to 1, 100, 500, and 5000 s^{-1} for the black, dotted, dashed, and sphere-marker traces, respectively. As k_{cb2} increases, the magnitude of the cathodic peak current density for DMFc$^+$ transfer increases from −48 μA cm^{-2}, at a k_{cb2} of 1 s^{-1}, to −880 μA cm^{-2}, at k_{cb2} equal to 5000 s^{-1}. This is owing to the increased availability of the metal ion to catalyze the DMFc-H$^+$ formation. However, similar to the effect observed in Figs. 4C and 5, during the reverse scan, from roughly 0.550 to −0.200 V, the current density decays gradually owing to the flux of OH$^-$ across the interface. Fig. 6 serves to demonstrate the importance of ion-pair formation to the catalytic behaviour of the metal ion, as well as its impact on the overall mechanism.

Fig. 7 illustrates the simulated CVs obtained through iterative changes in $k_{chem\text{-}2}$, such that the $k_{chem\text{-}2}$ equal to 1×10^2 L mol^{-1} s^{-1} (solid trace) and 1×10^8 L mol^{-1} s^{-1} (spherical marker trace) demonstrates only a minute change in the DMFc$^+$ transfer peak intensity, from −2.03 to −2.06 μA cm^{-2}. Analogously, the rates of

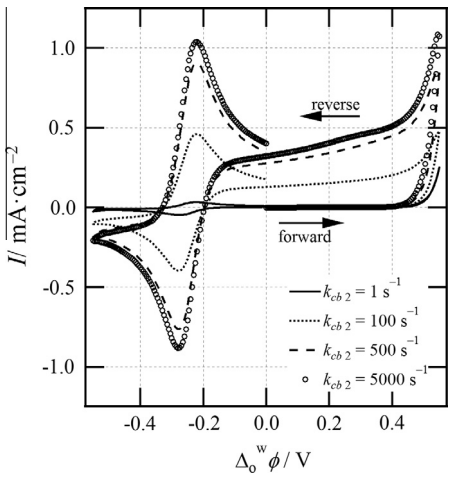

Fig. 6. Simulated cyclic voltammograms generated using the same parameters as those described for Fig. 4; however, $k_{cf} = 1 \times 10^2$ L mol^{-1} s^{-1} and $k_{cf2} = 5000$ - L mol^{-1} s^{-1}, were employed whilst varying k_{cb2} as indicated, inset.

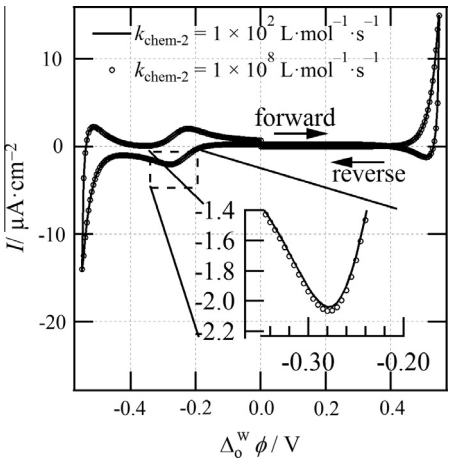

Fig. 7. Cyclic voltammograms generated using the simulation outlined in Section 2 comprised of similar parameters as those described for Fig. 4; however, $k_{cf} = 1 \times 10^2$ L mol^{-1} s^{-1}, $k_{chem\text{-}1} = 1 \times 10^4$ L mol^{-1} s^{-1}, along with $k_{chem\text{-}3}$ and $k_{chem\text{-}4} = 1 \times 10^2$ L mol^{-1} s^{-1}, were used while $k_{chem\text{-}2}$ was changed as listed, inset. The inset graph displays a magnified region of the two traces for the DMFc$^+$ transfer cathodic waves.

$k_{chem\text{-}3}$ and $k_{chem\text{-}4}$ were also varied systematically (data not shown) and elicited similar results to those found for $k_{chem\text{-}2}$. This seems to suggest that reaction **1** (k_{cf}/k_{cb}) and **2** ($k_{chem\text{-}1}$) have the largest influence on the CV profile, with further reactions having less impact on the response.

Eq. (vi) offers another parameter for optimization in that the ratio of the forward and reverse rate constants of reaction **1** can be altered while keeping the overall complexation constant, $K = k_{cf}/k_{cb}$, the same. In this way, K was maintained at 1×10^4 and the ratios of k_{cf}/k_{cb} were set equal to $1 \times 10^2/1 \times 10^{-2}$, $1 \times 10^4/1$, $1 \times 10^8/1 \times 10^4$ L mol^{-1} s^{-1} for Fig. S1 panels A, B, and C, respectively. The homogeneous rate constants of reactions **2** to **5** were maintained at 1×10^4 L mol^{-1} s^{-1}. The response is similar to that observed in Fig. 4; this is likely owing to the general consumption of species through the later reactions, thereby facilitating the forward directional dominance of reaction **1**.

DFc and Fc were also explored as possible electron donors and compared to DMFc using Cell 1 with 10 mM of LiOH in the aqueous; experimental CVs are shown in Fig. 8. The half-wave IT potentials for DFc$^+$ and Fc$^+$ were determined to be roughly

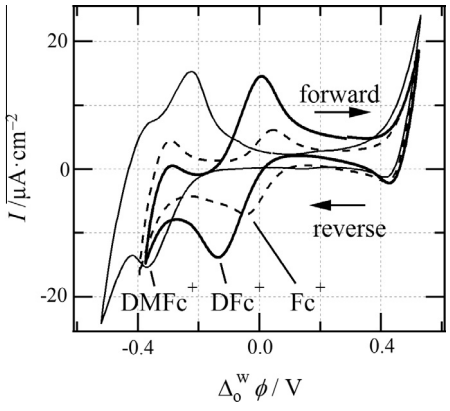

Fig. 8. Cyclic voltammograms (CVs) measured using Cell 1 with 'Fc deriv.' as DMFc, DFc, and Fc for the thin, thick, and dashed curves, respectively; the ion transfer peaks for the oxidized forms of the electron donor species are indicated. Similar instrument parameters as those detailed for Fig. 2 have been used in the acquisition of these CVs.

−0.065 and 0.000 V, respectively. Based on the rate constants evaluated thus far, it is possible to estimate the rates of reaction **1** and **2** for the three electron donor species. DMFc and DFc elicit comparable $DMFc^+/DFc^+$ cathodic IT peak current densities, at roughly −15.4/−13.8 μA cm^{-2}, along with similar Li^+ return peak intensities, at −1.3/−2.2 μA cm^{-2}; therefore, k_{cf} and $k_{chem\text{-}1}$ were both approximated to be 100 L mol^{-1} s^{-1}. In the case of Fc, if the diffusion coefficients of these three species are considered to be roughly equivalent, then amount of Fc^+ is half that of DMFc or DFc. Based on this, Fc was considered to yield between 50 and 100 L mol^{-1} s^{-1} for reaction **1** and 100 L mol^{-1} s^{-1} for **2**. In this way, a general trend in reactivity for these ferrocene derivatives can be proposed to be DMFc > DFc > Fc, that is in good agreement with the recent results reported by Samec et al. [28]. In that submission [28], the authors demonstrate an increasing rate of both the catalyzed and Fc derivative only mediated O_2 reduction with increasing methyl substitution on the cyclopentadienyl rings. Additionally, the rates estimated here are in good agreement with those found by Samec et al. [28] using stopped-flow kinetic measurements.

Other alkali and alkali earth metals, such as Na^+, K^+, and Mg^{2+} along with transition metals such as Zn^{2+} and Fe^{3+} were attempted; however, a great deal of current density oscillation was encountered in the CVs, although appreciable amounts of $DMFc^+$ was generated (data not shown). This oscillation is likely owing to the 'Marangoni effect', recently explored through cation transfer at a large ITIES by Kakiuchi et al. [60], and is the result of species adsorbed at the interface. The presence of $DMFc^+$ is promising and, combined with this instability, may indicate a trend towards a predominately interfacial versus bulk mechanism. Unfortunately, the analysis of the resultant CVs proved difficult and alternative methods, including liquid|liquid electrochemistry at a micro-ITIES, are being explored; however, this is beyond the scope of the present article.

5. Conclusions

The mechanism of oxygen reduction in a biphasic – between water and an organic solvent, in this case DCE – was investigated voltammetrically employing only lithium hydroxide as analyte/supporting electrolyte in the aqueous phase, along with DMFc, DFc, or Fc as an electron donor in DCE. Simulated voltammograms, generated using COMSOL Multi-physics software, were used to investigate the impact of different reaction rates within a proposed mechanism on the CV curve features and then compared to those seen experimentally. The proposed mechanism included the potential dependent IT of Li^+, OH^-, and $DMFc^+$, along with six homogeneous organic phase reactions. Reaction **1** involved a proton abstraction by DMFc from the hydration sphere of the metal ion forming DMFc-H^+ and the metal ion-hydroxide ion-pair. It was proposed that the metal ion would transfer either with some of its hydration sphere intact or it would transfer into hydration 'pockets' already present in the DCE phase as has been previously shown [7,29]. In this way, the metal ion behaves as a Lewis acid, weakening the O—H bonds of the water molecules surrounding it and, thus, water becomes the proton source.

Reactions **2** to **6** follow the typical pathway [7,20,25,28], such that the DMFc-hydride then reacts with one equivalent of oxygen to form $DMFc^+$ and a hydrogen peroxyl radical species. This radical can then oxidize DMFc and form HO_2^-, which can either disproportionate or, similar to reaction **1**, abstract a proton from a water molecule in the metal ions hydration shells to form H_2O_2.

By systematically varying the rates of these reactions it has been demonstrated herein, that reactions **1** and **2** play the dominant role. The rates of these two reactions were estimated to be ca. 100 L mol^{-1} s^{-1} for both **1** and **2** for DMFc and DFc electron donors, while for Fc these were estimated to be between 50 and 100 L mol^{-1} s^{-1} for **1** and 100 L mol^{-1} s^{-1} for **2**. Because **1** and **2** were found to exert the greatest influence on the CV profile it is not possible to establish a clear estimate of the rates of reactions **3** to **6**; however, it is generally accepted that radical reactions are fast (reaction **3**) and it has been shown here that the ion-pair formation can have a dramatic influence.

The method presented herein offers a new avenue with which to explore the Lewis acid properties of various metal ions. This approach could offer critical insight into the development of new catalysts for hydrogen fuel cells, whose presence has been shown to enhance performance [32], as well as offer routes to investigate their reactivity of novel synthetic methodologies [7].

Conflict of interest

The authors declare no conflict of interest.

Acknowledgements

We gratefully acknowledge the helpful discussions with and technical assistance of Manuel A. Méndez, Micheál D. Scanlon, Heron Vrubel, Jonnathan C.A. Hidalgo, and Lucie Rivier along with the generous assistance of Patricia Byron-Exarcos. HD is thankful to the China Scholarship Council (CSC) for financial support. This research was supported by the Polish-Swiss Research Programme, Project PSPB-035/2010: "Electrocatalysis at droplets".

Appendix A. Supplementary material

Supplementary data can be found online and includes a Table S1: COMSOL parameters, Fig. S1, and COMSOL 4.4 Model Report. Supplementary data associated with this article can be found, in the online version, at http://dx.doi.org/10.1016/j.jelechem.2014.07.040.

References

[1] S. Proch, M. Wirth, H.S. White, S.L. Anderson, J. Am. Chem. Soc. 135 (2013) 3073–3086.
[2] D.A. Walsh, A. Ejigu, J. Smith, P. Licence, Phys. Chem. Chem. Phys. 15 (2013) 7548–7554.
[3] J. Lee, K. Murugappan, D.W.M. Arrigan, D.S. Silvester, Electrochim. Acta 101 (2013) 158–168.
[4] J.-M. Noël, Y. Yu, M.V. Mirkin, Langmuir 29 (2013) 1346–1350.
[5] A. Trojánek, J. Langmaier, H. Kvapilová, S. Záliš, Z. Samec, J. Phys. Chem. A 118 (2014) 2018–2028.
[6] T.J. Stockmann, H. Deng, P. Peljo, K. Kontturi, M. Opallo, H. Girault, J. Electroanal. Chem. (2014) (submitted for publication).
[7] H. Deng, P. Peljo, T.J. Stockmann, L. Qiao, T. Vainikka, K. Kontturi, M. Opallo, H.H. Girault, Chem. Commun. 50 (2014) 5554–5557.
[8] K. Mittra, S. Chatterjee, S. Samanta, A. Dey, Inorg. Chem. 52 (2013) 14317–14325.
[9] S. Fukuzumi, K. Ohkubo, T. Suenobu, Acc. Chem. Res. 47 (2014) 1455–1464.
[10] P. Hapiot, C. Lagrost, Chem. Rev. 108 (2008) 2238–2264.
[11] A. René, D. Hauchard, C. Lagrost, P. Hapiot, J. Phys. Chem. B 113 (2009) 2826–2831.
[12] S. Fukuzumi, K. Okamoto, C.P. Gros, R. Guilard, J. Am. Chem. Soc. 126 (2004) 10441–10449.
[13] D.J. Fermín, Z. Ding, H.D. Duong, P.-F. Brevet, H.H. Girault, J. Phys. Chem. B 102 (1998) 10334–10341.
[14] C. Shi, F.C. Anson, Inorg. Chem. 37 (1998) 1037–1043.
[15] H.A. Gasteiger, N.M. Marković, Science 324 (2009) 48–49.
[16] M. Lefèvre, E. Proietti, F. Jaouen, J.-P. Dodelet, Science 324 (2009) 71–74.
[17] W. Nam, Y.-M. Lee, S. Fukuzumi, Acc. Chem. Res. 47 (2014) 1146–1154.
[18] M. Kasuno, A. Uehara, N. Ichieda, T. Kitano, K. Banu, S. Kihara, J. Electroanal. Chem. 579 (2005) 223–237.
[19] A. Trojánek, J. Langmaier, Z. Samec, Electrochem. Commun. 8 (2006) 475–481.
[20] B. Su, R.P. Nia, F. Li, M. Hojeij, M. Prudent, C. Corminboeuf, Z. Samec, H.H. Girault, Angew. Chem. Int. Ed. 47 (2008) 4675–4678.
[21] A. Trojánek, J. Langmaier, B. Su, H.H. Girault, Z. Samec, Electrochem. Commun. 11 (2009) 1940–1943.
[22] B. Su, I. Hatay, P.Y. Ge, M. Mendez, C. Corminboeuf, Z. Samec, M. Ersoz, H.H. Girault, Chem. Commun. 46 (2010) 2918–2919.

[23] P. Peljo, T. Rauhala, L. Murtomäki, T. Kallio, K. Kontturi, Int. J. Hydrogen Energy 36 (2011) 10033–10043.
[24] H. Deng, P. Peljo, F. Cortés-Salazar, P. Ge, K. Kontturi, H.H. Girault, J. Electroanal. Chem. 681 (2012) 16–23.
[25] P. Peljo, L. Murtomäki, T. Kallio, H.-J. Xu, M. Meyer, C.P. Gros, J.-M. Barbe, H.H. Girault, K. Laasonen, K. Kontturi, J. Am. Chem. Soc. 134 (2012) 5974–5984.
[26] N.A. Kotov, M.G. Kuzmin, J. Electroanal. Chem. 338 (1992) 99–124.
[27] B. Su, I. Hatay, F. Li, R. Partovi-Nia, M.A. Méndez, Z. Samec, M. Ersoz, H.H. Girault, J. Electroanal. Chem. 639 (2010) 102–108.
[28] A. Trojánek, J. Langmaier, Z. Samec, Electrochim. Acta 82 (2012) 457–462.
[29] P. Sun, F.O. Laforge, M.V. Mirkin, J. Am. Chem. Soc. 129 (2007) 12410–12411.
[30] Y.-X. Xie, R.-Y. Tang, R.-J. Song, J.-N. Xiang, J.-H. Li, J. Org. Chem. 79 (2013) 686–691.
[31] Y. Deng, S. Kumar, H. Wang, Chem. Commun. 50 (2014) 4272–4284.
[32] J. Park, Y. Morimoto, Y.-M. Lee, W. Nam, S. Fukuzumi, Inorg. Chem. 53 (2014) 3618–3628.
[33] M. Trombetta, N.E. Williams, S. Fischer, A. Gokirmak, H. Silva, Electron. Lett 50 (2014) 100–101.
[34] S. Matar, J. Ge, H. Liu, J. Power Sources 243 (2013) 195–202.
[35] J. Xiao, M. Hu, P. Bénard, R. Chahine, Int. J. Hydrogen Energy 38 (2013) 13000–13010.
[36] J.S. Bell, B.J. Lewis, Nucl. Eng. (Inst. Nucl. Eng.) 250 (2012) 134–141.
[37] D. Zigah, A. Wang, C. Lagrost, P. Hapiot, J. Phys. Chem. B 113 (2009) 2019–2023.
[38] T.J. Stockmann, Z. Ding, Can. J. Chem. (2014).
[39] T.J. Stockmann, Z. Ding, J. Phys. Chem. B 116 (2012) 12826–12834.
[40] E.J.F. Dickinson, H. Ekström, E. Fontes, Electrochem. Commun. 40 (2014) 71–74.
[41] P.J. Rodgers, S. Amemiya, Anal. Chem. 79 (2007) 9276–9285.
[42] T.J. Stockmann, A.-M. Montgomery, Z. Ding, J. Electroanal. Chem. 684 (2012) 6–12.
[43] A.J. Bard, L.R. Faulkner, Electrochemical Methods: Fundamentals and Applications, 2nd ed., John Wiley, New York, 2001.
[44] J.E.B. Randles, Trans. Faraday Soc. 44 (1948) 327–338.
[45] P. Peljo, H.H. Girault, Electrochemistry at Liquid/Liquid Interfaces. Encyclopedia of Analytical Chemistry, John Wiley & Sons Ltd, 2012.
[46] Z. Samec, J. Langmaier, T. Kakiuchi, Pure Appl. Chem. 81 (2009) 1473–1488.
[47] H. Girault, Electrochemistry at Liquid-Liquid Interfaces, in: A.J. Bard, C.G. Zoski (Eds.), Electroanalytical Chemistry, CRC Press, 2010, pp. 1–104.
[48] K. Zhurov, E.J.F. Dickinson, R.G. Compton, J. Phys. Chem. B 115 (2011) 6909–6921.
[49] A.J. Parker, Electrochim. Acta 21 (1976) 671–679.
[50] T. Wandlowski, V. Mareček, Z. Samec, Electrochim. Acta 35 (1990) 1173–1175.
[51] A.J. Olaya, M.A. Méndez, F. Cortes-Salazar, H.H. Girault, J. Electroanal. Chem. 644 (2010) 60–66.
[52] T.J. Kealy, P.L. Pauson, Nature 168 (1951) 1039–1040.
[53] J. Mähler, I. Persson, Inorg. Chem. 51 (2012) 425–438.
[54] H. Girault, Analytical and Physical Electrochemistry, 1st ed., EPFL Press, Lausanne, CH, 2004.
[55] C. Wohlfarth, Permittivity (Dielectric constant) of Liquids, in: CRC Handbook of Chemistry and Physics, CRC Press, Boca Raton, FL, 2011, pp. 6–186.
[56] A. Molina, E. Torralba, C. Serna, J.A. Ortuño, Electrochim. Acta 106 (2013) 244–257.
[57] Z. Samec, D. Homolka, V. Mareček, J. Electroanal. Chem. Interfacial Electrochem. 135 (1982) 265–283.
[58] Y. Shao, M.D. Osborne, H.H. Girault, J. Electroanal. Chem. Interfacial Electrochem. 318 (1991) 101–109.
[59] Y. Kitazumi, T. Kakiuchi, Bull. Chem. Soc. Jpn. 84 (2011) 1312–1320.
[60] T. Kasahara, N. Nishi, M. Yamamoto, T. Kakiuchi, Langmuir 20 (2004) 875–881.